Wind and Structures, *Vol. 23, No. 6 (2016) 559-575*
DOI: http://dx.doi.org/10.12989/was.2016.23.6.559

Wind loads and load-effects of large scale wind turbine tower with different halt positions of blade

Shitang Ke[*1,2], Wei Yu[1a], Tongguang Wang[1b], Lin Zhao[2c] and Yaojun Ge[2d]

[1]*Jiangsu Key Laboratory of Hi-Tech Research for Wind Turbine Design, Nanjing University of Aeronautics and Astronautics, Nanjing 210016, China*
[2]*State Key Laboratory for Disaster Reduction in Civil Engineering, Tongji University, Shanghai 200092, China*

(Received December 26, 2015, Revised January 15, 2016, Accepted October 28, 2016)

Abstract. In order to investigate the influence of different blade positions on aerodynamic load and wind loads and load-effects of large scale wind turbine tower under the halt state, we take a certain 3 MW large scale horizontal axis three-blade wind turbine as the example for analysis. First of all, numerical simulation was conducted for wind turbine flow field and aerodynamic characteristics under different halt states (8 calculating conditions in total) based on LES (large eddy simulation) method. The influence of different halt states on the average and fluctuating wind pressure coefficients of turbine tower surface, total lift force and resistance coefficient, circular flow and wake flow characteristics was compared and analysed. Then on this basis, the time-domain analysis of wind loads and load-effects was performed for the wind turbine tower structure under different halt states by making use of the finite element method. The main conclusions of this paper are as follows: The halt positions of wind blade could have a big impact on tower circular flow and aerodynamic distribution, in which Condition 5 is the most unfavourable while Condition 1 is the most beneficial condition. The wind loads and load-effects of disturbed region of tower is obviously affected by different halt positions of wind blades, especially the large fluctuating displacement mean square deviation at both windward and leeward sides, among which the maximum response occurs in 350° to the tower top under Condition 8; the maximum bending moment of tower bottom occurs in 330° under Condition 2. The extreme displacement of blade top all exceeds 2.5 m under Condition 5, and the maximum value of windward displacement response for the tip of Blade 3 under Condition 8 could reach 3.35 m. All these results indicate that the influence of halt positions of different blades should be taken into consideration carefully when making wind-resistance design for large scale wind turbine tower.

Keywords: wind turbine tower; blade position; large eddy simulation; aerodynamic load; wind-induced response

1. Introduction

Large scale wind turbine tower system belongs to the typical high rise and wind sensitive

∗Corresponding author, Associate professor, E-mail: keshitang@163.com
[a] Postgraduate, E-mail: yuweinuaa@163.com
[b] Professor, E-mail: tgwang@nuaa.edu.cn
[c] Professor, E-mail: zhaolin@tongji.edu.cn
[d] Professor, E-mail: yaojunge@tongji.edu.cn

http://www.techno-press.org/?journal=was&subpage=8 ISSN: 1226-6116 (Print), 1598-6225 (Online)

structure, and its tower-blade coupling structure possesses the features of complex wind field, small damping ratio, low vibration frequencies and so on (Jeong, Kim *et al*. 2013, Karimirad and Moan 2011, Germanischer Lloyd 2010). Therefore wind load becomes one of the main loads in tower structural design. Since the external loads on wind turbine tower is mainly determined by surrounding wind conditions, wind turbine will be shut down under high speed wind conditions and the different halt positions will cause the difference between flow field and aerodynamic distribution of tower surface, thus leading to the different wind loads and load-effects. Therefore, the research for wind loads and load-effects of large scale wind turbine tower under different halt positions could pave a path for further wind-resistance design under high wind speed conditions.

In earlier studies on wind-resistance performance of the wind turbine tower (Duquette and Visser 2003, Tempel 2006, Agarwal and Manuel 2009), the wind turbine system was simplified as a single degree of freedom system to obtain the dynamic characteristics and single wind vibration coefficient, which could not accurately reveal the characteristics of aerodynamic loads and wind-induced responses. Currently, the research work focus on wind load and wind-induced response of large scale wind turbine tower structure is more complicated. Tran and Wang (Tran, Kim *et al*. 2015, Wang, Zhang *et al*. 2013) employed harmony superposition method and CFD(Computational Fluid Dynamics) numerical simulation method to simulate time histories of normal wind and typhoon respectively, and made static and dynamic response analysis for wind turbine tower structure under both normal wind and typhoon conditions. They found that there exists a big difference for the wind-induced response characteristics of tower between the typhoon and normal wind conditions. The tower is the most prone to yield failure when suffering from a sudden 90° deflected typhoon. Hoogedoorn and Binh (Hoogedoorn, Jacobs *et al*. 2010, Binh, Ishihara *et al*. 2008) investigated the peak factor distribution of non-Gaussian wind-induced response for this wind turbine tower structure. They came up with peak factor expression in third order, considering the components of wind speed spatial correlation, wind-induced background and resonant response. Ke, Yu and Kwon (Ke, Wang *et al*. 2015, Yu and Kwon 2014, Kwon, Kareem *et al*. 2012) employed modified blade element-momentum theory and finite element time domain analysis method to analyze the wind-induced response characteristics of large scale wind turbine tower-blade system, taking both SSI and aeroelastic effects into consideration. Their work indicated that SSI effect could increase the average and fluctuating response of tower structure significantly, while the aeroelastic could decrease wind-induced dynamic response notably, especially under high speed wind conditions, for which the reduction could be up to 15%. Wang and Griffith (Wang, Hansen *et al*. 2015, Griffith, Carne *et al*. 2008) revealed the aerodynamic load characteristics and vibration mechanism of MW-level wind turbine tower-blade coupling system and discussed the effects of blade rotation and centrifugal force on wind-induced response of the system. Most research works are aimed at aerodynamic numerical simulation and wind vibration response analysis of large scale wind turbine under fixed blade conditions currently, however, few of them are involved in aerodynamic force and wind loads and load-effects of wind turbine tower structure under different halt states.

For this reason, this paper takes a 3 MW large scale horizontal axis three-blade wind turbine as an example for further analysis. Numerical simulation was conducted for wind turbine tower-blade system under different halt states (8 calculating conditions in total, determined by the overall process of blade rotating condition and the relative position of tower) based on LES method at the beginning and the aerodynamic force based time history of typical points of tower and blade surfaces were obtained as input parameters for subsequent wind loads and load-effects analysis. Dynamic characteristic and time-domain analysis of wind loads and load-effects for the wind

turbine tower-blade coupling model under different halt states were then performed, making use of the finite element method. Finally, the influence of different halt states on the flow field characteristics, aerodynamic force distribution, and the wind loads and load-effects of large scale wind turbine system was compared and studied. Based on these results, the most favourable and unfavourable blade halt positions of large scale wind turbine system under strong wind conditions were summarized.

2. Project Profile

Taking a selected 3MW horizontal axis three-blade wind turbine as example, the detailed parameters are given as follows: the height of the tower was 85 m, the radius of the top of the tower was 2.0 m and the radius of the bottom of the tower was 2.5 m; the tower was linked variable-thickness structure with a thickness of the top wall of 30 mm and the bottom wall, 60 mm; the cut-in wind speed was 3.5 m/s, rated wind speed was 12.5 m/s, the cut-out wind speed was 25 m/s and the tilt angle of the wind turbine was 5°; the angle between each blade was 120° and the blades were evenly distributed along the circumference; the length of the blade was 44.5 m and the detailed parameters of each blade element section along the wingspan are given in Table 1. The dimension of the engine room was 12 m × 4 m × 4 m (length × width × height). Components such as blades, engine room and wheel hub were established in sequence according to the above design parameters and the 3D tower-blade model of large scale wind turbine was built by Boolean calculation, as shown in Fig. 1.

Fig. 1 The 3D model of a large scale wind turbine system

Table 1 Parameters of wind turbine blades

Position %	Radius r	Chord length C	Inflow angle φ	Pitch angle β
5	2.225	2.561	0.823	37.140
10	4.450	4.646	0.640	26.672
15	6.675	4.389	0.507	19.069
20	8.900	3.808	0.414	13.692
25	11.125	3.228	0.346	9.830
30	13.350	2.738	0.296	6.976
35	15.575	2.313	0.258	4.802
40	17.800	1.970	0.229	3.103
45	20.025	1.686	0.205	1.742
50	22.250	1.448	0.186	0.630
55	24.475	1.246	0.169	-0.293
60	26.700	1.074	0.156	-1.072
65	28.925	0.925	0.144	-1.736
70	31.150	0.796	0.134	-2.310
75	33.375	0.682	0.125	-2.810
80	35.600	0.582	0.118	-3.250
85	37.825	0.492	0.111	-3.640
90	40.050	0.412	0.105	-3.987
95	42.275	0.340	0.099	-4.299
100	44.500	0.275	0.095	-4.580

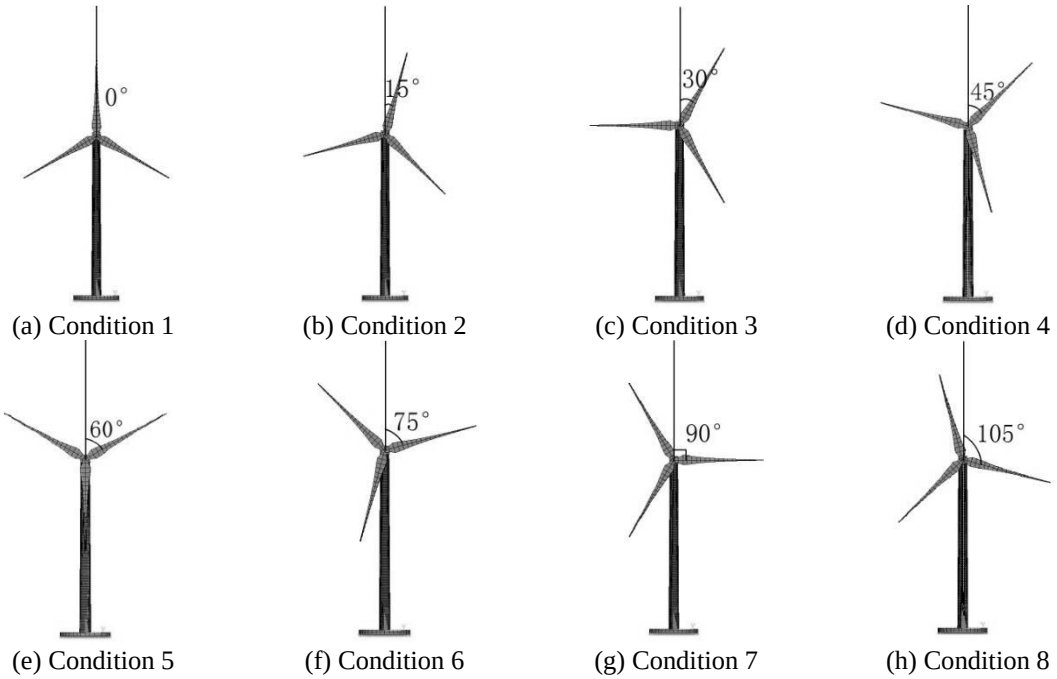

(a) Condition 1 (b) Condition 2 (c) Condition 3 (d) Condition 4

(e) Condition 5 (f) Condition 6 (g) Condition 7 (h) Condition 8

Fig. 2 The diagram of finite element under different calculate conditions

According to the relative position of the blade and tower, with consideration of the periodicity during the rotation of three-blade system, a total of eight calculating conditions were setup with an initial state of 0° between the blade and vertical direction with an increment 15° of along clockwise direction. The specific positions are demonstrated in Fig. 2.

3. CFD numerical simulation

3.1 Calculating domain and meshing

In order for the flow to completely develop, the calculating domain was taken as 12D × 5D × 5D (flow direction x × span-wise direction × vertical direction, D is the diameter of blade rotation). The wind turbine was setup at a distance of 3D to the entry of the calculating domain to ensure that the wake flow can fully develop in 8D. Due to the complexity of the blade surface, hybrid mesh discrete mode was used and the complete calculating domain was divided into two parts, where the core region was meshed by tetrahedron and local mesh around the wind turbine was encrypted, while the outer region was meshed by fine hexahedron mesh. The wall y plus in the current simulation is 38.3. The total number of mesh was 7.95 million. The calculating domain and details of meshing are shown in Fig. 3.

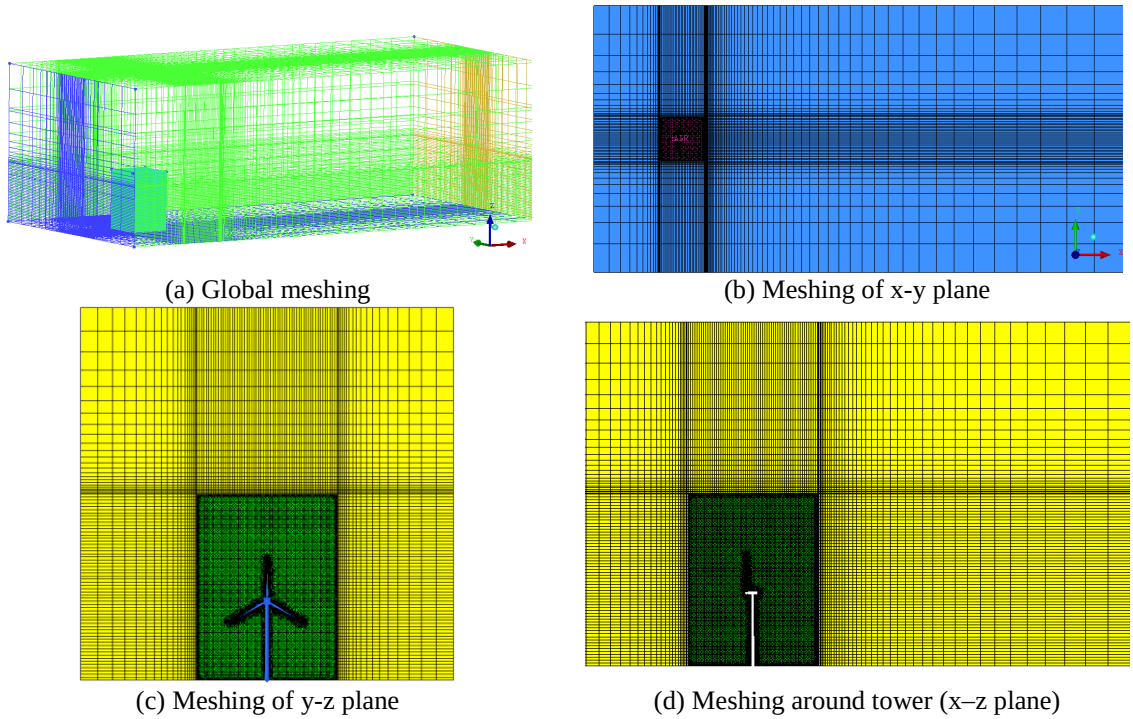

(a) Global meshing

(b) Meshing of x-y plane

(c) Meshing of y-z plane

(d) Meshing around tower (x–z plane)

Fig. 3 Schematic diagram of the calculating domain and encrypted meshing

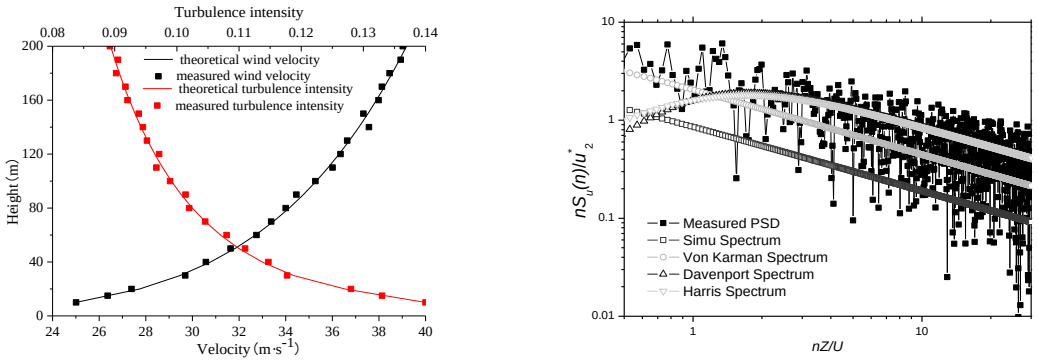

(a) Vertical and turbulence profiles (b) Fluctuating wind power spectrums

Fig. 4 Comparison of Simulation parameters between LES and the measured results

3.2 Boundary conditions and turbulence model

The boundary condition of the entry was defined as velocity entry in which the ground roughness coefficient of the wind velocity section was 0.15 and the basic wind velocity at a reference height of 10 m was 25 m/s. The distribution form with respect to type B geologic conditions in China was used for the turbulence strength section. The connection of boundary condition of inflow and FLUENT were realized by user-defined function, and wind velocity profile and turbulence intensity profile were imposed in the simulation (as shown in Fig. 4). The boundary condition of the exit was defined as pressure exit with a relative pressure of 0. Non-slipping surface was used for the ground of the calculating domain and the surface of the wind turbine, and symmetric boundary conditions were used for the side and the top surfaces of the calculating domain.

3D single precision discrete solver was used in numerical calculation. Due to the flow field where the wind turbine located was unsteady constant and the condition of turbulence flow was complex, the complicated flow field of wind turbine can be better simulated by LES (Hoogedoorn, Jacobs *et al*. 2010, Jiménez, Crespo *et al*. 2010). Smagorinsky-Lilly model was used for sub-grid scale and the pressure-velocity coupling equation sets were solved by SIMPLEC format which has good convergence and is suitable for LES calculation with small time step (Zuo and Kang 2014). Least Squares Cell Based method was used for gradient, and standard format was used for the pressure. Bounded Central Differencing format was used for momentum, and Second Order Upwind was used for energy and Second Order Implicit was used for transient formulation. The residual difference of calculation of control equations was 0.000001. The correlation characteristics of time must be analysed by time step Δt, and it can be roughly estimated by the ratio of the size of local grid Δx and the characteristic of flow velocity, time step is set as 0.001s in this paper.

4. The aerodynamic performance

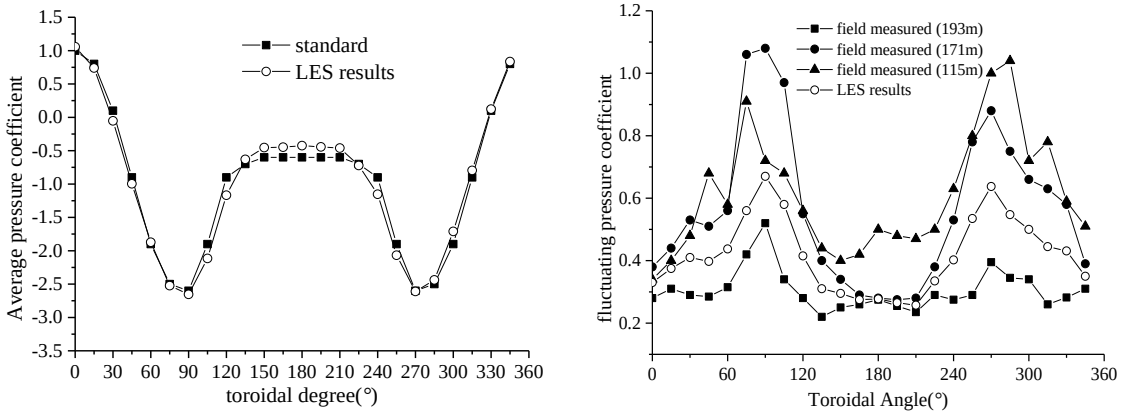

(a) Average wind pressure coefficients (b) Fluctuating wind pressure coefficients

Fig. 5 Comparison of aerodynamic loads for wind turbine tower with LES and the measured results

4.1 Validity checking

In order to verify the correction of simulation method for wind turbine tower-blade system, Fig. 5 shows the distribution of average pressure coefficient and fluctuating wind pressure coefficient of the typical cross section which was less affected by blades, and these compared with the standard and the measured distribution curve (Li, Tao *et al.* 2015, GB50009-2012 2012, Nishimura and Taniike 2001) both at home and abroad.

The results show that the distribution of average wind pressure coefficient by the large eddy simulation is almost same as given by standard, especially the values on the windward, and only the values on the leeward face are slightly less than standard values, which could be caused by the aerodynamic interference from blades. More specifically, only wind pressure distribution of cylindrical section is given by standard, actually the wind turbine tower is significantly affected by blades, and this is main reason why the value of numerical simulation is different from standard values. The fluctuating wind pressure distribution curve is among the measured curve at home and abroad, and the distribution trend with circumference is relatively close. However, taking into consideration that the fluctuating wind pressure distribution are closely related to the terrain of the measured tower, inflow turbulence and the surrounding disturbances, the fluctuating wind pressure distribution trend and values were obtained by LES both in the envelope of the measured results, the comparison demonstrates that the simulating method of aerodynamic performance for wind turbine in this paper is accurate and steady.

4.2 Turbulence characteristics of turbine tower

According to the different disturbance from upstream blade wake that downstream tower suffered from under different working conditions, the tower was divided into section with less interference (0-40 m) and section with larger interference (40-85 m). Figs. 6 and 7 show the velocity contour distribution with streamlines of both tower sections with less and larger interference under different conditions. It is demonstrated that in the tower section without obvious interference, inflow turbulence won't be obstructed directly by the upstream blades and will

separate at the windward point of tower even under different working conditions. The lateral turbulence separation point is almost the same as well. Besides, reflux and vortex at different scales could happen on the leeward face of tower under different conditions. In the tower section with large interference, however, the interference effects between blades and tower become more dominant with the increase of coverage of blades on tower, which could be attributed to the divergent tower turbulence characteristics caused by the different relative position of upstream blades to the tower. Inflow turbulence without blade interference will flow to the downstream area directly; otherwise it will separate with the interference. The separated turbulence will flow along the blade surface and vortex will be formed at the leeward side of blades from the turbulence passing through both front and back part of blades. Small scale vortex could be formed near the blade surface and may become large scale vortex far away. The separation point at windward side of tower will deviate with the interference of blades, when the blades are moving close to the tower gradually.

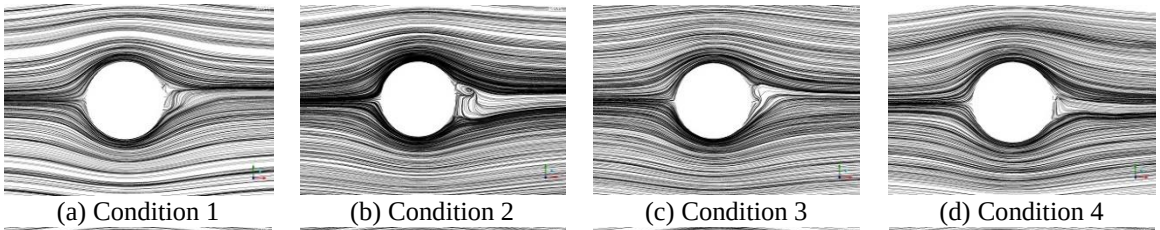

(a) Condition 1 (b) Condition 2 (c) Condition 3 (d) Condition 4

(e) Condition 5 (f) Condition 6 (g) Condition 7 (h) Condition 8

Fig. 6 Velocity contour with streamlines of tower with less interference section under different conditions

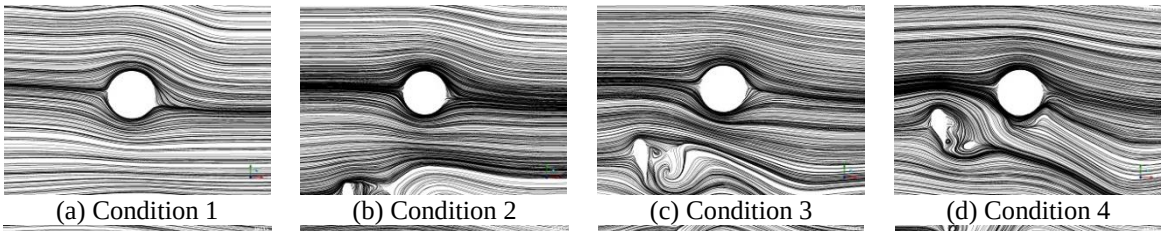

(a) Condition 1 (b) Condition 2 (c) Condition 3 (d) Condition 4

(e) Condition 5 (f) Condition 6 (g) Condition 7 (h) Condition 8

Fig. 7 Velocity contour distribution with streamlines of tower interference section under different conditions

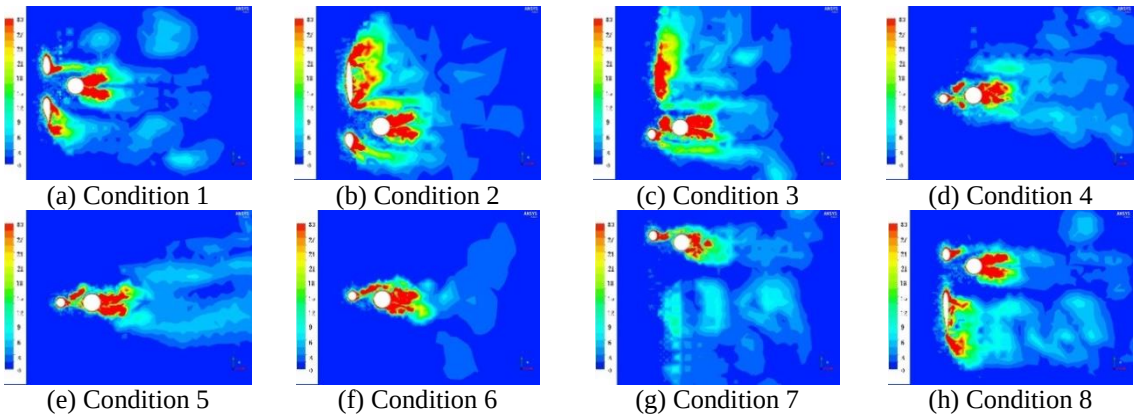

(a) Condition 1 (b) Condition 2 (c) Condition 3 (d) Condition 4

(e) Condition 5 (f) Condition 6 (g) Condition 7 (h) Condition 8

Fig. 8 Vorticity distribution of the wind turbine tower under different working conditions

Fig. 8 gives the vorticity distribution of the wind turbine tower under different working conditions. As shown in the figure, the interference effects between blades and tower will cause large scale increase in vorticity area of wind turbine system. The vorticity distributions of different blade halt positions are quite different. The blades are closer towards the tower, more evident the wake vortex at the back side of tower. Meanwhile, different relative positions of blades and tower would give rise to different wake vortex. The existence of tower could break the blade wake vortex and blade wake vortex could also change the shape of tower vortex. When the inflow turbulence is passing through the tower, there will be an obvious increase of flow speed surrounding the tower. This accelerating phenomenon is more remarkable if blades are even closer to the tower.

4.3 Characteristics of pressure coefficient distribution

We arranged 8 layer of measuring points uniformly in the meridian direction, 24 points in each circular direction and 12 points in the wingspan direction of each blade. Based on the Large Eddy Simulation (LES), we obtained the history curve of surface aerodynamics of wind turbine system as subsequent input parameters for the calculation of wind-induced dynamic response in time domain. Due to limited content, Fig. 9 only presents the history curve of pressure coefficient of typical points of blades and tower section without obvious interference under Condition 1.

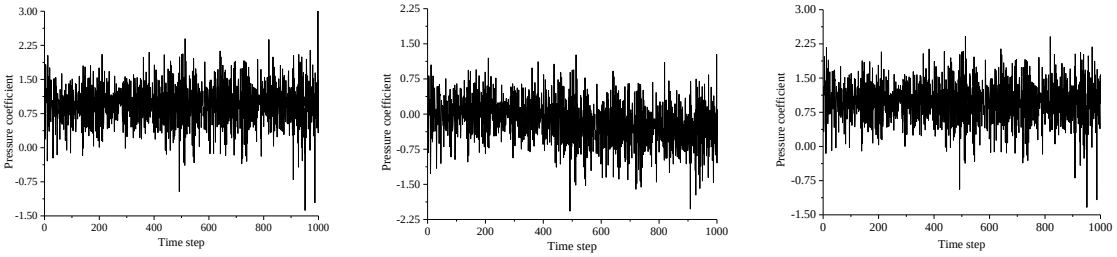

(a) windward side of tower (b) leeside of tower (d) windward side of blade

Fig. 9 The history curve of pressure coefficient of wind turbine typical points

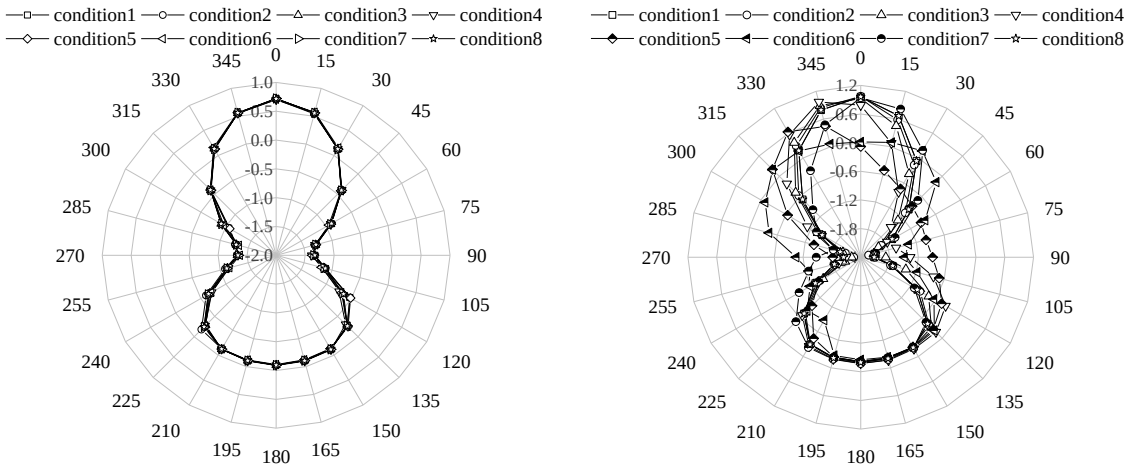

(a) less disturbed tower section (b) disturbed tower section

Fig. 10 Pressure coefficient distribution of the wind turbine tower under different working conditions

The coverage of shapes induces the change of wake flow of tower and the variation between tower and blades. The disappearance of vortex will make a difference on the distribution of pressure coefficient at tower surface. Fig. 10 shows the average pressure coefficient distribution of wind turbine tower under different working conditions. We draw the conclusions as below:

i. The pressure coefficient distribution trends along the circular cross section of less disturbed tower section are consistent and symmetric under different working conditions. Since there is no interference on tower in the direction of inflow turbulence, positive pressure zone is always present at ±30° region of windward side of tower. And the pressure coefficient reaches the maximum value of around 0.8 at the windward side. Negative pressure zone is present at bilateral sides and leeward side of tower and the negative pressure of bilateral sides are much higher than that of leeward side.
ii. Significant difference of pressure distribution is present due to the different coverage of blades on tower in the direction of inflow turbulence of the disturbed section. The pressure distribution under the condition without obvious interference is similar to the circular distribution of undisturbed section. The pressure coefficient of windward side will increase with the increase of height and coverage area.
iii. Negative pressure zone is present at shaded region of windward side of tower. Negative pressure decreases with the increase of coverage area and the circular pressure coefficient distribution is unsymmetrical. There exists a reducing tendency for negative pressure due to the blades interference at both sides. The influence of different blade positions on the leeward side of tower is very tiny.

4.4 Lift and drag coefficient distribution

In order to analyse the blade interference effects on the lift and drag coefficient distribution on the tower cross section. Fig. 11 shows an instantaneous distribution of lift coefficients and drag

coefficients of the wind turbine tower under different working conditions, and Table 2 shows the ratios of lift coefficients and drag coefficients at different height of tower under different conditions. Therefore, we can draw the conclusions:

i. The lift coefficient of tower cross section below 40 m is almost lower than the drag coefficient under different working conditions, while this phenomenon is opposite above 40 m.
ii. With the increase of blade coverage on tower in the direction of inflow turbulence, lift coefficient will become much larger than drag coefficient.
iii. The maximum difference between lift and drag coefficient occurs under Condition 5, in which tower is totally covered by the blades and negative pressure zone is present at shaded region of windward side of tower. Meanwhile the Fluctuating wind is increased in this condition. For the cross section of tower at a height of 60 m, the lift coefficient reaches 5.864 times of drag coefficient. This indicates that it is necessary to consider the influence of lift coefficient on the wind-resistance design when the wind turbine tower is under halt states.

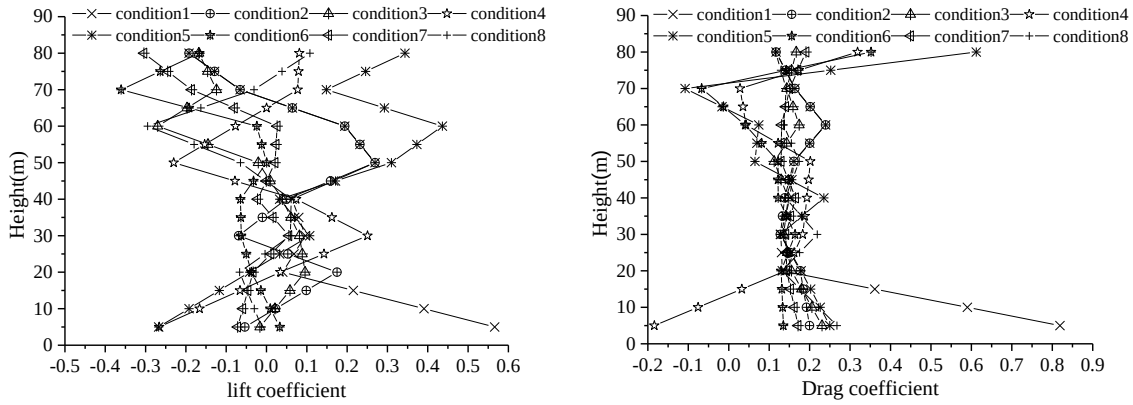

(a) lift coefficient (b) drag coefficient

Fig. 11 Lift and drag coefficient distribution of the wind turbine tower under different working conditions

Table2 The list of lift and drag coefficients ratios at different height of tower under different conditions

cl/cd	Working Conditions							
	Cond. 1	Cond. 2	Cond. 3	Cond. 4	Cond. 5	Cond. 6	Cond. 7	Cond. 8
10 m	0.662	0.117	0.102	2.188	-0.850	0.071	-0.363	-0.137
20 m	0.304	0.990	0.616	0.245	-0.234	-0.290	-0.231	-0.508
30 m	0.748	-0.541	0.602	1.370	0.838	-0.382	0.392	0.271
40 m	0.419	0.352	0.267	0.381	0.139	-0.528	-0.135	0.436
50 m	1.672	1.671	-0.182	-1.142	4.781	0.002	0.163	-0.371
60 m	0.811	0.811	-1.548	-1.803	5.864	-0.589	0.202	-2.172
70 m	-0.401	-0.401	-0.865	2.755	-1.377	5.377	-1.233	-0.218
80m	-1.641	-1.642	-1.005	0.256	0.561	-0.473	-1.592	0.931

Table 3 The list of first 300 order frequency comparison of wind turbine under different conditions

mode	Cond. 1	Cond. 2	Cond. 3	Cond. 4	Cond. 5	Cond. 6	Cond. 7	Cond. 8
1st	0.209	0.209	0.209	0.208	0.208	0.208	0.209	0.209
5th	0.466	0.466	0.467	0.467	0.467	0.467	0.467	0.466
10th	1.450	1.452	1.455	1.459	1.460	1.459	1.455	1.452
20th	3.753	3.751	3.748	3.747	3.746	3.747	3.749	3.751
30th	6.935	6.934	6.930	6.926	6.925	6.926	6.930	6.934
50th	16.010	16.010	16.010	16.010	16.010	16.010	16.010	16.010
100th	31.602	31.605	31.609	31.612	31.613	31.612	31.609	31.606
200th	55.472	55.472	55.472	55.472	55.472	55.472	55.472	55.472
300th	72.756	72.756	72.756	72.756	72.756	72.756	72.756	72.756

5. The wind load and load-effects

5.1 Dynamic characteristic analysis

The wind turbine tower-blade integrated finite element model under different working conditions was established based on ANSYS platform, among which SHELL 63 element used for tower and blades and BEAM 188 element stimulated for the cabin. Besides, SOLID 65 was used as basic unit for circular raft foundation, with 24 m in diameter and 2 m in height. The bottom of foundation was fixed and the relationship between the ground and foundation was simulated by COMBINE 14 spring element. Each portion of wind turbine was combined into tower-blade integrated finite element model through multi-point unit coupling. The total model was divided into 6485 units based on the principles of efficiency and accuracy.

Table 3 shows typical intrinsic frequency of wind turbine calculated and extracted by Lanczos method. It is found that the fundamental frequency of blades-tower coupled wind turbine system is quite low even under different conditions, only about 0.209 Hz. And the frequency interval between each mode is very small. The different halt positions of blades mainly influence the low-order intrinsic frequency, and some minor differences are found under different working conditions. While the high-order frequency remains almost the same. As for the frequency and vibration mode of wind turbine system, the influence of halt positions is much smaller. For the low-order mode, cabin and tower are driven to wave and swing by the blades; for the high-order mode, the structure deformation and instability of tower and blades may occur.

5.2 Characteristics of wind loads and load-effects

The wind loads and load-effects in time domain was calculated based on ANSYS software platform; wind pressure coefficient was obtained by LES method as wind load input parameters; the transient dynamics balance equation was solved by implicit Newmark and HHT integration method. The damping value of each mode is 0.02; integration time step is 0.05 s; loading time steps are 6000; basic wind speed is regarded as 25 m/s and peak factor is 2.5. (Ke, Wang *et al.* 2015)

Fig. 12 shows the radial displacement of mean response of tower under different calculating conditions, in which negative value means radial inside and vice versa. The mean radial displacement distributions of tower are consistent under different working conditions, and the

influence of different blade positions are primarily focus on the upper portion of tower. The radial displacement increases gradually with the increase of tower height. Both the biggest positive and negative displacements appear at 350° and 170° to the tower top. The biggest displacement under Condition 6 is 0.193 m and the smallest displacement under Condition 2 is 0.133 m.

Fig. 13 shows root mean square (RMS) of radial displacement responses of tower under different calculating conditions. Trailing vortex of blade will be changed because of different relative position between blade and tower, meanwhile the existence of the tower destroyed the blade trailing vortex, and the blade trailing vortex will also change the shape of the tower of vortex.

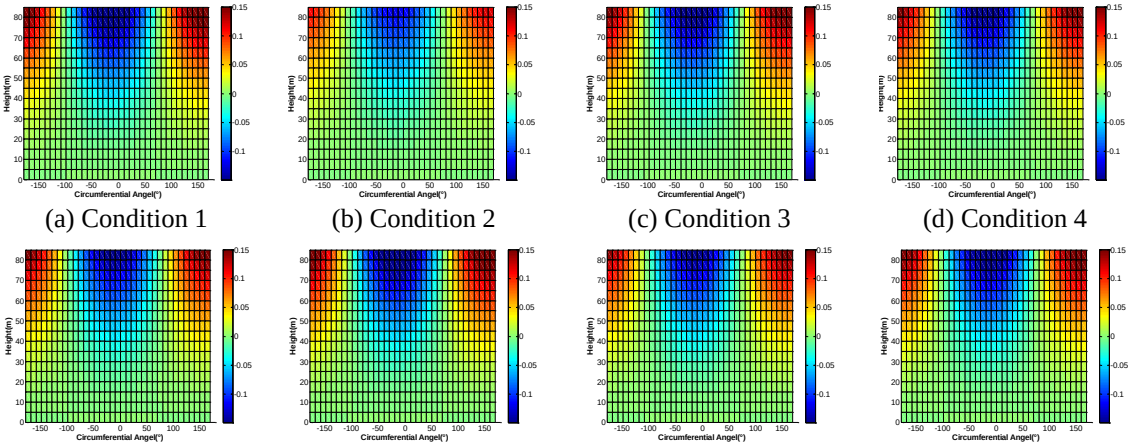

(a) Condition 1 (b) Condition 2 (c) Condition 3 (d) Condition 4

(e) Condition 5 (f) Condition 6 (g) Condition 7 (h) Condition 8

Fig. 12 The radial displacement of mean response of tower under different calculating conditions

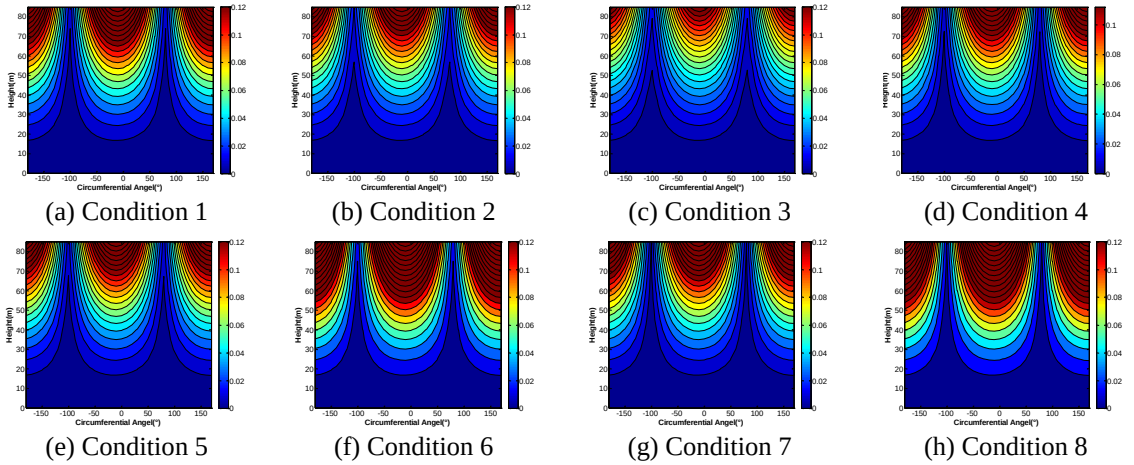

(a) Condition 1 (b) Condition 2 (c) Condition 3 (d) Condition 4

(e) Condition 5 (f) Condition 6 (g) Condition 7 (h) Condition 8

Fig. 13 RMS of radial displacement response of tower under different calculating conditions

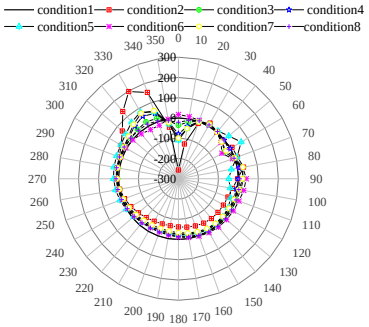

(a) mean circular bending moment

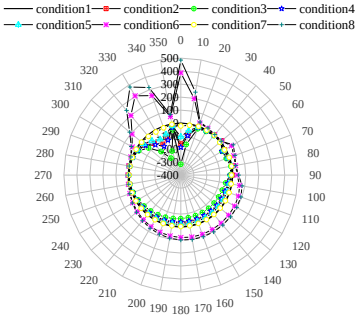

(b) RMS of circular bending moment

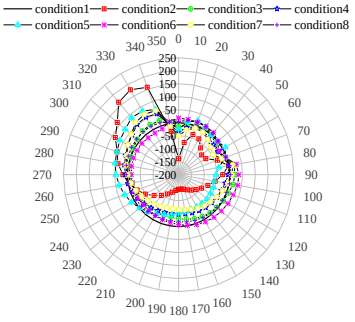

(c) mean vertical bending moment

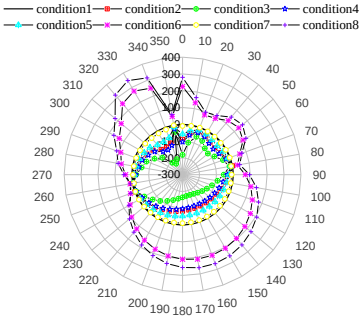

(d) RMS of vertical bending moment

Fig. 14 Characteristic force responses of tower bottom under different calculating conditions

The root mean square of radial displacement response increases with the increase of height, the dominant mutual interference between upper blades and tower leads to two peak value regions at windward and leeward side. The minimum value of root mean square of radial displacement response is at a height of 80 m under Condition 3, while the maximum value appears at a height of 55 m under Condition 8.

In order to compare the effects of different blade halt positions on the bending characteristics of tower bottom, we set the response under Condition 1 as the initial state, and the force values under other working conditions were calculated for the difference. Fig. 14 shows characteristic force responses of tower bottom under different calculating conditions. By comparing these figures, it reveals that:

i. The mean circular bending moment at tower bottom shows the difference at 0°, 60°, 90° and 330°, and the maximum difference is at 0° under Condition 2, up to 256.93 N·m.
ii. The mean vertical bending moments under Condition 2 and 5 are quite different, while the biggest difference lies in 330° under Condition 2.
iii. The increase of root mean square of bending moment fluctuating response at tower bottom is the most remarkable at 0° and 330° under Condition 6 and Condition 8.

Table 5 The list of peak displacements of blades top under different working conditions

Type of displacement		Cond. 1	Cond. 2	Cond. 3	Cond. 4	Cond. 5	Cond. 6	Cond. 7	Cond. 8
Blade 1 (m)	Peak	-2.47	-1.70	-1.78	-1.92	-2.58	-2.23	-1.50	-2.14
	RMS	0.70	0.57	0.45	0.53	0.48	0.66	0.42	0.69
Blade 2 (m)	Peak	-1.17	-1.32	-0.73	-0.98	-2.53	-1.06	-0.99	-1.34
	RMS	0.32	0.41	0.18	0.29	0.21	0.31	0.29	0.41
Blade 3 (m)	Peak	-1.25	-1.44	-1.20	-1.78	-2.58	-2.74	-2.24	-3.35
	RMS	0.36	0.42	0.29	0.50	0.48	0.82	0.65	1.06

Table 4 shows the characteristics of blade root force under different working conditions. The different halt positions cause great difference in blade root force. The mean shear force and bending moment both decrease if the blades are closer to the tower. The mean force reaches maximum under Condition 1 and minimum under Condition 5; the mean square deviation of fluctuating response reaches the highest value under Condition 2 and Condition 8.

We defined the blade with a vertical tilt angel of 0° as No.1, and No.2 and No.3 were set in clockwise successively. Table 5 shows peak displacement of blade top under different working conditions. From the table, it is found that the maximum negative value of each blade could reach beyond -2.50 m under Condition 5, while the displacement value of each blade is smaller under Condition 3. The maximum negative value of single blade may be above -2.00 m under other working conditions, among which the maximum value occurs at the top of Blade 3 under Condition 8. Different halt positions of Blade 2 may have shading effect on tower, which is the most notable under Condition 5. The maximum negative displacement could reach -2.530 m, and the mutual interference between blades and tower gets stronger at that time. Therefore, different positions of blades would lead to accordingly huge displacement difference at blade top. So we advise to take into consideration of peak displacement at blade top under the most unfavourable halt states when making wind-resistance design for turbine tower.

6. Conclusions

In summary, we systematically investigated the effects of different halt states on the flow field, aerodynamic distribution and wind-induced vibration characteristics of wind turbine tower system based on LES and finite element method. The major conclusions are as follows:

- The windward points of inflow turbulence and lateral separation points in the less disturbed region of tower are fixed under different working conditions, but the scale and range that vortex falls off at leeward side maybe slightly different. The different positions of upstream blades will lead to the divergence flow at tower region with obvious disturbances, and when the blades are moving closer to the tower, the separation point at windward side is blocked and caused to deviate by the blades. The vortex scale and fall-off region markedly increase and the wake region at the back side of tower becomes slim and irregular.
- The tendencies of circular pressure coefficient distribution of tower section with less disturbances are consistent and symmetrical, and drag coefficient is much larger than lift coefficient. Negative pressure zone may exist in covered region of tower windward side.

What's more, the lift coefficient could surpass the drag coefficient with the decrease of negative pressure caused by the increase of covering area. The lift coefficient reaches the maximum value at a height of 60 m under Condition 5.

- The different blade halt positions have minor influence on the frequency and vibration mode of wind turbine–blade system. For low-order mode, the blades are driven to wave and swing; for high-order mode, large structure deformation and instability are found on both tower and blades.
- The different blade halt positions could strongly influence the radial displacement responses in the upper portion of tower. The most evident displacement response takes place under Condition 6, and the maximum displacement was appeared at the top of tower under different conditions. There are two peaks of mean square deviation of fluctuating displacements in windward and leeward side. The difference of bending moment characteristics of tower bottom becomes prominent at 0° and 330° in circular direction. Among them, the mean value turns most remarkable under Condition 2 and Condition 5, while fluctuating response gets most remarkable under Condition 6 and Condition 8.
- Shear force and bending moment characteristics of blade root tend to decrease when the tower is getting closer to blades. The extreme displacement of blade top could reach beyond 2.50 m for all the three blades under Condition 5. The maximum blade top displacement of 3.35 m comes out under Condition 8.

Acknowledgments

This work was jointly funded by the National Basic Research Program of China ("973" Program) under Grant No. 2014CB046200, open fund for Jiangsu Key Laboratory of Hi-Tech Research for Wind Turbine Design (ZAA1400206), and China Postdoctoral Science Foundation (2015T80551), and Jiangsu Outstanding Youth Foundation (BK20160083).

References

Agarwal, P. and Manuel, L. (2009), "Simulation of offshore wind turbine response for long-term extreme load prediction", *Eng. Struct.*, **31**(10), 2236-2246.

Binh, L.V., Ishihara, T., Phuc, P.V. et al. (2008), "A peak factor for non-Gaussian response analysis of wind turbine tower", *J. Wind Eng. Ind. Aerod.*, **96**(10-11), 2217-2227.

China Classification Society (2008), Code for wind turbines, Beijing, China.

Djojodihardjo, H., Hamid, M.F.A., Jaafar, A.A., Basri, S., Romli, F.I., Mustapha, F., Mohd Rafie, A.S. and Abdul Majid, D.L.A. (2013), "Computational study on the aerodynamic performance of wind turbine airfoil fitted with Coanda jet", *J. Renew. Energ.*, **2013**(2013).

Duquette, M.M. and Visser, K.D. (2003), "Numerical implications of solidity and blade number on rotor performance of horizontal-axis wind turbines", *J. Solar Energy Eng.*, **125**(4), 425-432.

GB 50009-2012, Load code for the design of building structures. (2012), The Ministry of Structure of the People's Republic of China, Beijing. (in Chinese)

Germanischer Lloyd (2010), Guideline for the certification of wind turbines, *Hamburg: Germanischer Lloyd*.

Griffith, T.D., Carne, T.G. and Paquette, J.A. (2008), "Modal testing for validation of blade models", *Wind Eng.*, **32**(2), 91-102.

Hoogedoorn, E., Jacobs, G.B. and Beyene, A. (2010), "Aero-elastic behavior of a flexible blade for wind turbine application: A 2D computational study", *Energy*, **35**(2), 778-785.
Jeong, M.S., Kim, S.W., Lee, I. et al. (2013), "The impact of yaw error on aeroelastic characteristics of a horizontal axis wind turbine blade", *Renew. Energ.*, **60**, 256-268.
Jiménez, Á., Crespo, A. and Migoya, E. (2010), "Application of a LES technique to characterize the wake deflection of a wind turbine in yaw", *Wind Energy*, **13**(6), 559-572.
Karimirad, M. and Moan, T. (2011), "Wave-and wind-induced dynamic response of a spar-type offshore wind turbine", *J. Waterw. Port C - ASCE*, **138**(1), 9-20.
Ke, S,T., Cao, J.F., Wang, L. and Wang, T.G. (2014), "Time-domain analysis of the wind-induced responses of the coupled model of wind turbine tower-blade coupled system", *J. Hunan university(Natural Sciences)*, **41**(4), 87-93. (in Chinese)
Ke, S.T., Ge, Y.J., Wang, T.G., Cao, J.F. and Tamura, Y. (2015), "Wind field simulation and wind-induced responses of large wind turbine tower-blade coupled structure", *Struct. Des. Tall. Spec.*, **24**(8), 571-590
Ke, S.T., Wang, T.G., Ge, Y.J. and Tamura, Y. (2015), "Aeroelastic responses of ultra large wind turbine tower-blade coupled structures with SSI effect", *Adv. Struct. Eng.*, **18**(12), 2075-2087.
Kwon, D.K., Kareem, A. and Butler, K. (2012), "Gust-front loading effects on wind turbine tower systems", *J. Wind Eng. Ind. Aerod.*, **104**(3), 109-115.
Lee, K.S., Huque, Z. and Han, S E. (2015), "A study on the y+ effects on turbulence model of unstructured grid for CFD analysis of wind turbine", *J. Korean Assoc. Spatial Struct.*, **15**(1), 75-84.
Li, C.F., Tao, X.J., Li, H.G. and Zhang, J.L. (2012), "Modeling and analyzing freedom feather of wind turbine", *Adv. Mater. Res.*, **512-515**, 739-742.
Li, X., Lu, Y., Liu, Q. et al. (2015), "Experimental study on wind-included interference effects of circular section chimneys", *Eng. Mech.*, **1**, 159-162. (in Chinese)
Nishimura, H. and Taniike, Y. (2001), "Aerodynamic characteristics of fluctuating forces on a circular cylinder", *J. Wind Eng. Ind. Aerod.*, **89**(1), 713-723.
Tempel, J.V.D. (2006), "Design of support structures for offshore wind turbines", *Netherlands: Delft University of Technology*.
Tran, T.T., Kim, D.H. and Nguyen, B.H. (2015), "Aerodynamic interference effect of huge wind turbine blades with periodic surge motions using overset grid-based computational fluid dynamics approach", *J. Solar Energy Eng.*, **137**(6), 061003.
Wang Z.Y., Zhang, B., Zhao, Y. et al. (2013), "Dynamic response of wind tuebine under typhoon", *Acta Energiae Solaris Sinica*, **34**(8), 1434-1442. (in Chinese)
Wang, K., Hansen, M. and Moan, T. (2015), "Model improvements for evaluating the effect of tower tilting on the aerodynamics of a vertical axis wind turbine", *Wind Energy*, **18**(1), 91-110.
Yu, D.O. and Kwon, O.J. (2014), "Predicting wind turbine blade loads and aeroelastic response using a coupled CFD–CSD method", *Renew. Energ.*, **70**(5), 184-196.
Zuo, W. and Kang, S. (2014), "Numerical simulation of the aerodynamic performance of a H-type wind turbine during self-starting", *Appl. Mech. Mater.*, **529**, 296-302.

CC